J. Phys.: Condens. Matter **22** (2010) 116005 (13pp) doi:10.1088/0953-8984/22/11/116005

Valence change and magnetic order in $YbMn_6Ge_{6-x}Sn_x$

T Mazet[1], H Ihou-Mouko[1], D H Ryan[2], C J Voyer[2], J M Cadogan[3] and B Malaman[1]

[1] Institut Jean Lamour, Département P2M, CNRS (UMR 7198)—Nancy Université, BP 70239, F-54506 Vandoeuvre-lès-Nancy Cedex, France
[2] Physics Department and Centre for the Physics of Materials, McGill University, Montreal, QC, H3A 2T8, Canada
[3] Department of Physics and Astronomy, University of Manitoba, Winnipeg, MB, R3T 2N2, Canada

Received 4 December 2009, in final form 20 January 2010
Published 5 March 2010
Online at stacks.iop.org/JPhysCM/22/116005

Abstract
The $YbMn_6Ge_{6-x}Sn_x$ compounds ($0 < x < 6$) have been investigated using x-ray diffraction, magnetic measurements, neutron diffraction and ^{170}Yb Mössbauer spectroscopy. The $YbMn_6Ge_{6-x}Sn_x$ system comprises three solid solutions: (i) $0 < x \leqslant 1.1$, (ii) $3.2 \leqslant x \leqslant 4.6$ and (iii) $5.3 \leqslant x < 6$, all of which crystallize in the hexagonal ($P6/mmm$) $HfFe_6Ge_6$-type structure. The substitution of Sn for Ge yields changes in the type of magnetic order (antiferromagnetic, helimagnetic, ferromagnetic, conical and ferrimagnetic), in the easy magnetization direction (from easy axis to easy plane) as well as in the valence state of Yb (from trivalent to divalent). The Mn moments order at or above room temperature, while magnetic ordering of the Yb sublattice is observed at temperatures up to 110 K. While Yb is trivalent for $x \leqslant 1.1$ and divalent for $x \geqslant 5.3$, both magnetic and ^{170}Yb Mössbauer spectroscopy data suggest that there is a gradual reduction in the average ytterbium valence through the intermediate solid solution ($3.2 \leqslant x \leqslant 4.6$), and that intermediate valence Yb orders magnetically, a very unusual phenomenon. Analysis of the ^{170}Yb Mössbauer spectroscopy data suggests that the departure from trivalency starts as early as $x = 3.2$ and the loss of ytterbium moment is estimated to occur at an average valence of ~2.5+.

1. Introduction

While most of the rare-earths are trivalent, some can occur in higher or lower valence states. Ytterbium in particular can occur as divalent, trivalent or with an intermediate valence [1, 2]. In its ground state, the isolated ytterbium atom is divalent ($4f^{14}$). In metallic solids, the 4f states of Yb can hybridize more or less strongly with other valence electrons (f–spd hybridization) [3, 4] to yield a complex electronic structure, which may give rise to exotic and fascinating physical phenomena such as heavy fermion, intermediate valence or Kondo effect [1, 2, 5, 6]. Hybridization with valence electrons may also lead to a stabilization of the trivalent state. The change in Yb valence is related to the exact location of a narrow peak of f character in the density of states which straddles the Fermi level [3, 4]. These continue to be topics of interest in solid state physics [7, 8].

When Yb is divalent ($4f^{14}$), as is the case in metallic Yb, it is non-magnetic ($J = 0$) and has an 'abnormally large' atomic radius compared to that of normal trivalent rare-earth elements [1, 2]. Divalent Yb behaves almost like an alkaline-earth element (e.g. Mg, Ca) [1]. In contrast, trivalent Yb has an atomic radius which follows the lanthanide contraction [1]. It is magnetic ($J = \frac{7}{2}$) and carries an effective moment close to the free ion value ($m_{\text{eff}} = 4.5\ \mu_B$). It can order magnetically at low temperatures: however, the ordered magnetic moment is often smaller than that of the free ion Yb^{3+} ($m = 4\ \mu_B$) [2, 8] due to crystal field effects. Ytterbium can also exhibit a valence state intermediate between divalent and trivalent [1, 2, 6]. In this situation, both the radius and the effective moment of the Yb ion may adopt intermediate values [6]. In a few rare cases, intermediate valence Yb ions can order magnetically [9, 10] and it then carries a reduced magnetic moment, but in most studied cases, if not all, Yb is alloyed with non-magnetic elements. In solids, the valence of Yb may be modified, slowly or abruptly, by external parameters such as temperature or pressure [1, 2, 6]. Increasing pressure generally stabilizes the smaller trivalent ytterbium

ion [7, 11]. Similarly, increasing temperature also tends to favour the trivalent state [12–14]. Chemical substitutions may also alter the Yb valence either through modification of the electronic structure, when the substituted and substituting atoms have different valence electronic configurations [15], or through chemical pressure effects, when the chemical species involved in the substitution have different atomic radii [16, 17].

Substituting Sn for Ge in $YbMn_6Ge_6$ should allow us to observe a Yb valence change. $YbMn_6Ge_6$ crystallizes in the hexagonal ($P6/mmm$) $HfFe_6Ge_6$-type structure with cell parameters close to those of $LuMn_6Ge_6$ [18, 19], pointing to trivalent (or nearly so) Yb. This pseudo-layered crystal structure, which comprises one Yb site (1b position), one Mn site (6i position) and three metalloid sites (in the 2c, 2d and 2e positions), can be described as an alternative stacking of two kinds of slab along the c axis: the Mn–Ge(2e)–Ge(2c)–Ge(2e)–Mn one (X-slab) and the Mn–[Yb,Ge(2d)] one (Yb-slab). Ytterbium is most likely divalent (or nearly so) in $YbMn_6Sn_6$, since its cell parameters are significantly larger that those of $LuMn_6Sn_6$ [20]. $YbMn_6Sn_6$ crystallizes in the $SmMn_6Sn_6$-type ($P6/mmm$) structure, a slightly disordered variant of the $HfFe_6Ge_6$-type structure that only occurs with the larger rare-earth elements [21, 22]. In this structural variant, a fraction ($\sim$25%) of the Yb and Sn(2e) atoms are shifted by $c/2$ from their ideal position in the $HfFe_6Ge_6$-type structure.

Studying the $YbMn_6Ge_{6-x}Sn_x$ system has two supplementary interests. First, it may lead to alloys where hybridized 4f states coexist with ordered 3d moments, an infrequent situation potentially rich in phenomena to explore. Second, the valence of Yb is expected to influence the Mn sublattice magnetic arrangement, well beyond the direct modifications that might result from the magnetic ordering of Yb (antiferromagnetic coupling between the Mn and Yb moments, magnetic anisotropy of Yb). The RMn_6X_6 (X = Ge or Sn) compounds show a systematic dependence of their magnetic properties on the R valence. When the rare-earth orders, all of the known magnetic structures are built from ferromagnetic Mn and R(001) planes [20, 23–27]. However, when the trivalent R is non-magnetic or is not magnetically ordered, the Mn sublattice always behaves antiferromagnetically (helimagnetism or collinear antiferromagnetism) [23–26]. For instance, from $T_N^{Mn} = 480$ K down to the magnetic ordering temperature of Yb at $T_t \sim 40$ K, $YbMn_6Ge_6$ adopts a collinear easy-axis antiferromagnetic arrangement (AF2) [19]. On the other hand, RMn_6X_6 (X = Ge or Sn) compounds with divalent R always exhibit easy-plane ferromagnetism, either over the whole magnetically ordered range in RMn_6Sn_6 (R = Mg, Ca, Yb) [20, 22] or over a wide temperature interval below the ordering temperature, as in $MgMn_6Ge_6$ [27]. Hence, based on these observations, trivalent Yb should not coexist with a ferromagnetic Mn sublattice in $YbMn_6Ge_{6-x}Sn_x$.

In this paper we study the $YbMn_6Ge_{6-x}Sn_x$ system by means of x-ray and neutron diffraction, magnetic measurements and ^{170}Yb Mössbauer spectroscopy. Section 2 describes the synthesis procedure and experimental techniques. The results are presented and discussed in section 3. We first describe the evolution in the crystal chemistry of this system based on Rietveld refinement of the x-ray data (section 3.1). We then determine the composition dependence of the magnetic properties and magnetic structures in section 3.2 before proceeding to analyse the ^{170}Yb Mössbauer spectra in section 3.3. Finally, a conclusion is given in section 4.

2. Synthesis and experimental details

The polycrystalline $YbMn_6Ge_{6-x}Sn_x$ samples were prepared from high-purity (at least 99.9%) commercially available elements. Due to the high vapour pressure of ytterbium metal at elevated temperatures, it is necessary to use a closed system to avoid excessive losses of Yb during the first thermal treatment. Hence, the starting materials were placed in Mo crucibles which were sealed by arc-welding in a glove box under a high-purity argon atmosphere. A supplementary inner glassy carbon crucible was used to avoid any reaction between Ge and the Mo wall. To prevent oxidation, the Mo crucibles were enclosed in silica tubes under purified argon (300 mm Hg) and then placed in a tube furnace. After a preliminary homogenization treatment of one week at 500 °C, the samples were ground, compacted and enclosed again before annealing for a further week at temperatures ranging from 700 °C (for the Ge-rich alloys with $x_{Sn} \leqslant 5.0$) to 650 °C (for the Sn-rich alloys with $x_{Sn} \geqslant 5.0$), since a lower annealing temperature tends to favour ordering of the Yb atoms within the slabs [21]. The compounds are stable in air for several months.

The precise Ge/Sn composition was determined by microprobe measurements (Cameca SX 100). Room temperature x-ray diffraction patterns were recorded using a Philips X'pert Pro Diffractometer ($\lambda_1 = 1.540\,56$ Å and $\lambda_2 = 1.544\,39$ Å). AC and DC magnetic measurements were performed using a PPMS (Quantum Design) apparatus between 5 and 350 K in DC magnetic fields of up to 5 T. A Manics DSM8 magneto-susceptometer was used for DC magnetization measurements in the 300–700 K temperature range. Some representative compositions were investigated using powder neutron diffraction at the Institut Laue Langevin (Grenoble, France) using the D1b two-axis diffractometer ($\lambda = 2.52$ Å, step of 0.2°). Several diffraction patterns were recorded in the 2–320 K temperature range using a standard helium cryostat.

Both the x-ray and neutron patterns were analysed using the Rietveld method with the Fullprof program [28]. Besides the peak profile parameters, the x-ray data refinements comprised scale factor, zero shift, cell parameters and crystallographic position parameters (z_{Mn} and $z_{Ge/Sn(2e)}$ and the Ge/Sn occupancy ratio for the three metalloid sites). For the neutron pattern refinements, the magnitude and orientation of the Mn and Yb magnetic moments were treated as additional free parameters but, to avoid an excessive number of intensity-dependent parameters, the Ge/Sn occupancy ratios were kept fixed to the values deduced from the x-ray data.

^{170}Yb Mössbauer measurements were made on a conventional cold-source spectrometer. A 20 mCi ^{170}Tm source was prepared by neutron activation of $\sim$25 mg of Tm as a 10 wt% alloy in aluminium. The source and sample were mounted vertically in a helium-flow cryostat and the drive was operated in sine mode. The 84.25 keV γ photons used for

^{170}Yb Mössbauer spectroscopy were isolated from the various x-rays emitted by the source using a high-purity Ge detector. Calibration of the spectrometer was achieved using a laser interferometer mounted on the back of the drive. Velocities were cross-checked against ^{57}Co/α-Fe at room temperature. A calibrated Cernox thermometer was used to monitor the sample temperature and a stability of better than ± 0.01 K was observed. The powder samples had areal densities of 1.0–1.5 g cm^{-2}, somewhat below optimum thickness given the low Yb content of the materials. Spectra were fitted using a nonlinear least-squares minimization routine with line positions and intensities derived from an exact solution to the full Hamiltonian [29].

3. Results and interpretation

3.1. Samples: composition and crystal chemistry

Our investigations have demonstrated the existence of two miscibility gaps in the $YbMn_6Ge_{6-x}Sn_x$ system. Both are marked by the presence of a mixture of two distinct 1-6-6 phases: one Ge-rich and the other Sn-rich. The first miscibility gap extends from about $x \sim 1.1$ up to about $x \sim 3.2$. This gap has also been observed in $RMn_6Ge_{6-x}Sn_x$ with normal trivalent R rare-earth elements [30] and will not be investigated further. The second one, which will be shown to be related to the valence change of Yb, is specific to the Yb-based system. Its borders, especially the Ge-rich one, depend on the annealing temperature. For example, a sample with nominal composition $x = 5.0$ annealed at 700 °C was found to be a $\frac{2}{3}$:$\frac{1}{3}$ mixture of $x \sim 4.6$ and $x \sim 5.3$ alloys, while a sample with the same initial composition annealed at 650 °C was found to be a 40:60 mix of $x \sim 4.3$ and $x \sim 5.4$ alloys. Because of the poor quality of the sample annealed at 700 °C, only the one annealed at 650 °C will be investigated here.

Room temperature x-ray data indicate that all of the compounds studied, even the Sn-rich phases, are isotypic with $HfFe_6Ge_6$ ($P6/mmm$). Since $YbMn_6Sn_6$ crystallizes in the partially disordered $SmMn_6Sn_6$-type structure, this shows that the Ge substitution favours the ordered distribution of Yb atoms within the slabs, as was also observed in $RMn_6Ge_2Sn_4$ with trivalent R [31]. Most samples were found to contain small amounts (not exceeding a few wt%) of the following impurities: Yb_2O_3, β-Sn, $MnSn_2$ and/or $Mn_5Ge_{3-x}Sn_x$. A few of the samples, especially the Ge-rich ones, had a higher content (up to ~10 wt%) of $Mn_5Ge_{3-x}Sn_x$.

The variation of the cell volume with composition is shown in figure 1. The continuous line, which links the volume of $YbMn_6Ge_6$ with that of $LuMn_6Sn_6$, corresponds approximately to the ideal behaviour (Vegard's law) expected if the Yb remained trivalent for all compositions. The dashed line, which links the cell volume of $YbMn_6Ge_6$ with that of $YbMn_6Sn_6$, corresponds to a simple linear variation of cell parameters. It is clear from figure 1 that the cell volume of $YbMn_6Ge_{6-x}Sn_x$ does not evolve linearly: the cell volumes in the Ge-rich terminal solid solution ($x \leqslant 1.1$) are visibly smaller than those predicted by either interpolation scheme, and those of the Sn-rich terminal solid solution ($x \geqslant 5.3$) lie

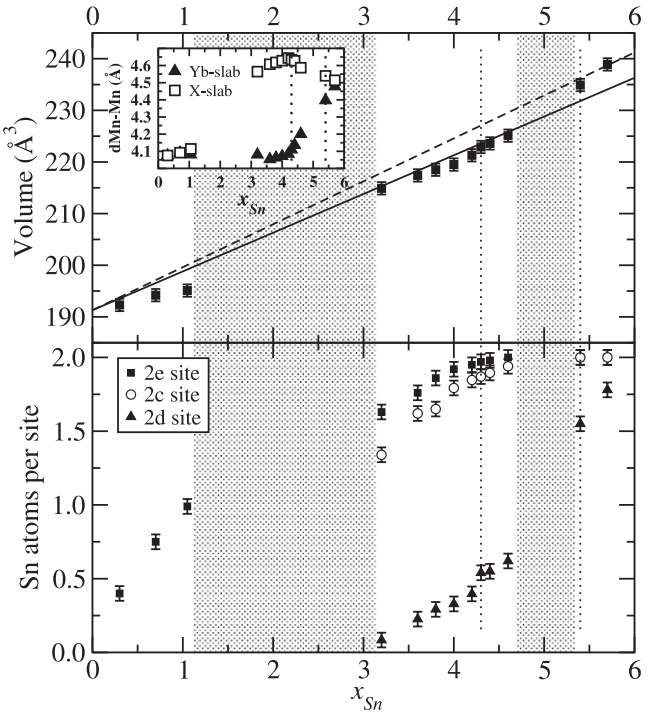

Figure 1. Composition dependence of (top) the room temperature cell volume and (bottom) the occupancy of the metalloid sites by Sn atoms in $YbMn_6Ge_{6-x}Sn_x$. The inset shows the evolution in the interplanar Mn–Mn distances through the Yb- and X-slabs. The shaded areas correspond to the two-phase regions. The vertical dotted lines mark compositions from the $x = 5.0$ two-phase sample.

well above the line expected for trivalent Yb. The evolution in the occupation of the three metalloid sites by Sn atoms is depicted in figure 1. In the Ge-rich concentration range ($x \leqslant 1.1$), the Sn atoms, being larger than the Ge atoms, exclusively occupy the 2e site, the largest of the three metalloid sites. It seems that the 2e sites are large enough to accommodate the Sn atoms with a limited expansion of the unit cell. For the intermediate solid solution ($3.2 \leqslant x \leqslant 4.6$), the cell volumes lie on the line expected for a trivalent Yb. In this concentration range, the 2e and 2c sites are almost full of Sn atoms while the smaller 2d site only starts to be substituted. As a result, the interlayer Mn–Mn distance through the X-slab is significantly larger than that through the Yb-slab (inset of figure 1), the latter being almost equal to that in $YbMn_6Ge_6$. A similar preferential occupation of the 2d site by Ge atoms occurs in $RMn_6Ge_2Sn_4$ with trivalent R [31–33]. In the Sn-rich solid solutions, the 2d site is finally occupied by Sn atoms and the interlayer distances through the Yb-slab strongly increase. Consequently, the 'chemical pressure' exerted on the Yb drops and the cell volumes shift onto the dashed line, suggesting that the Yb atoms are divalent for $x \geqslant 5.3$. This observation is consistent with the expectation that a larger volume available to the Yb atoms enhances the stability of the divalent state.

At this stage, it is very tempting to conclude that the Yb atoms in $YbMn_6Ge_{6-x}Sn_x$ are trivalent for $x \leqslant 4.6$ and divalent for $x \geqslant 5.3$ (i.e. in the Sn-rich terminal solid solution). Since it is not possible to synthesize $R_{1-x}R'_xMn_6Sn_6$ alloys involving R and R′ atoms of different valences [20], it would

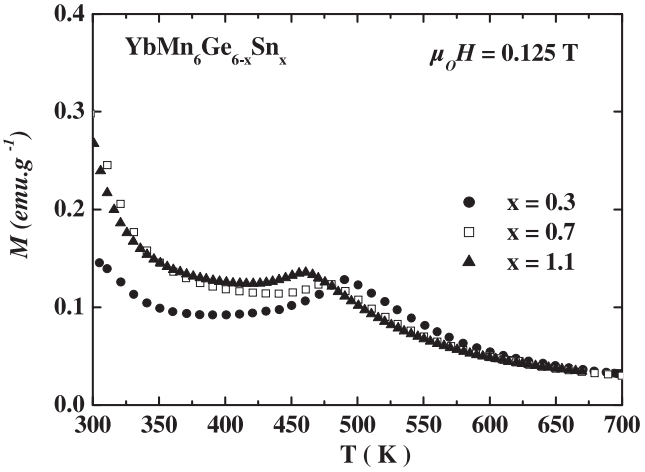

Figure 2. Temperature dependence of the magnetization of $YbMn_6Ge_{6-x}Sn_x$ ($x = 0.3$, 0.7 and 1.1) above room temperature.

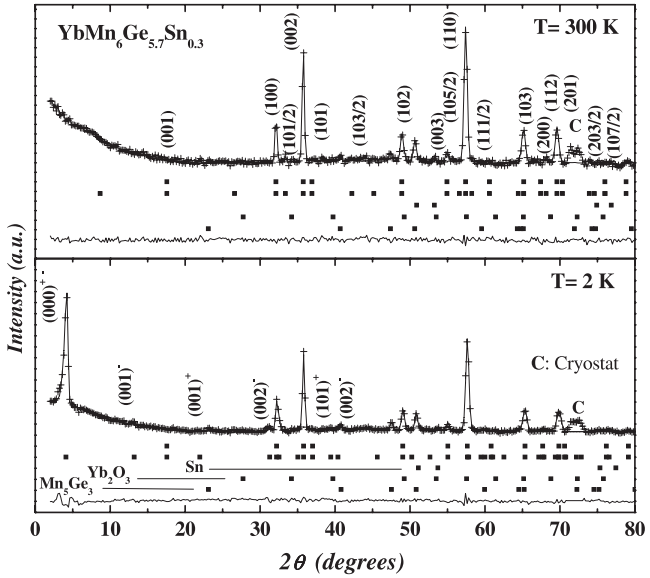

Figure 3. Neutron diffraction patterns of $YbMn_6Ge_{5.7}Sn_{0.3}$ at 300 and 2 K.

be tempting to associate the existence of the second miscibility gap with the effects of an abrupt shift in the ytterbium valence. However, as we show below, our magnetic measurements and ^{170}Yb Mössbauer spectra suggest a somewhat different scenario involving a more gradual variation of the Yb valence with Sn content.

3.2. Magnetic properties and magnetic structures

Depending on composition, four kinds of magnetic behaviour can be distinguished within the $YbMn_6Ge_{6-x}Sn_x$ system.

3.2.1. Alloys with $0 < x \leqslant 1.1$. The behaviour of the Ge-rich terminal solid solutions is similar to that of the $YbMn_6Ge_6$ end member, although the low temperature magnetic structure of this ternary compound is not yet precisely known.

The alloys order antiferromagnetically at high temperature and the transition temperature is found to decrease with increasing Sn content (figure 2), probably as a result of the increase in the Mn–Mn interatomic distances and the concomitant reduction in the strength of the exchange interactions. The low temperature dependence of the magnetization of these antiferromagnets is not presented here because it was overshadowed by a background from the ferromagnetic $Mn_5Ge_{3-x}Sn_x$ impurity (160 K $< T_C <$ 320 K) [34]. At both 300 and 5 K, the isothermal magnetization (not shown) shows no sign of a metamagnetic transition.

Neutron diffraction measurements were carried out on $YbMn_6Ge_{5.7}Sn_{0.3}$. From room temperature down to $T_t \sim 55$ K, the neutron diffraction patterns (figure 3) are characteristic of the easy-axis AF2 magnetic structure always observed for RMn_6Ge_6 involving non-magnetic or non-magnetically ordered trivalent R [23, 25, 26]. In addition to the nuclear reflections, a set of peaks of magnetic origin is observed. They can be indexed with a propagation vector $\mathbf{k} = \langle 0, 0, 1/2\rangle$, the $(00l/2)$ reflections being zero. In the AF2 magnetic structure, the magnetic cell is twice as large as the chemical one by doubling of the c axis (figure 4). The easy-axis ferromagnetic (001) Mn planes are stacked along the c axis with the $+--+$ sequence. At 300 K, the Mn moment refined to $m_{Mn} = 1.69(24)\ \mu_B$. Below $T_t \sim 55$ K, the $(hkl/2)$ magnetic lines disappear while a new set of magnetic satellites grows. The latter can be indexed with a propagation vector $\mathbf{k}' = \langle 0, 0, q_z\rangle$, with q_z being independent of temperature: $q_z \sim 0.24$ reciprocal lattice units (r.l.u.). Various kinds of possible magnetic arrangements have been tested. The best refinements (table 1) clearly show that the Yb sublattice is magnetically ordered. They indicate a conical structure, built out of ferromagnetic (001) Yb and Mn planes. In this conical structure, the Mn and Yb moments are globally antiferromagnetically coupled, as expected with a heavy rare-earth, and form a cone of half-angle α whose axis deviates from the [001] direction by an angle θ (see figure 4). The incommensurate magnetic moment components transverse to the cone axis describe a spiral. At 2 K, the refinements yield cone half-angles α of $\sim$60° and $\sim$120° for Mn and Yb, respectively. The cone axis deviates by $\theta \sim 65°$ from the c axis. From the refined phase angle φ and q_z values (table 1), the angle between the transverse component of the Mn moments of adjacent (001) layers can be deduced (see [25] for details). It is about $\sim$60° through the Yb-slab and about $\sim$90° through the X-slab. The transverse part of the Mn and Yb moments makes an angle of $\sim$150°. The magnetic moment magnitudes are refined to $m_{Mn} = 2.07(19)\ \mu_B$ and $m_{Yb} = 2.89(37)\ \mu_B$ at 2 K. The magnetic moment carried by Yb atoms is hence significantly below the Yb^{3+} free ion value ($gJ = 4$). This conical arrangement yields a weak spontaneous magnetization, which cannot be checked from our magnetic measurements due to the presence of the ferromagnetic $Mn_5Ge_{3-x}Sn_x$ impurity, but corresponds well with what is observed for $YbMn_6Ge_{6-x}Ga_x$ with low Ga content [35]. It is very likely that the as-yet unknown low temperature magnetic structure of $YbMn_6Ge_6$ [19] is similar to that described above.

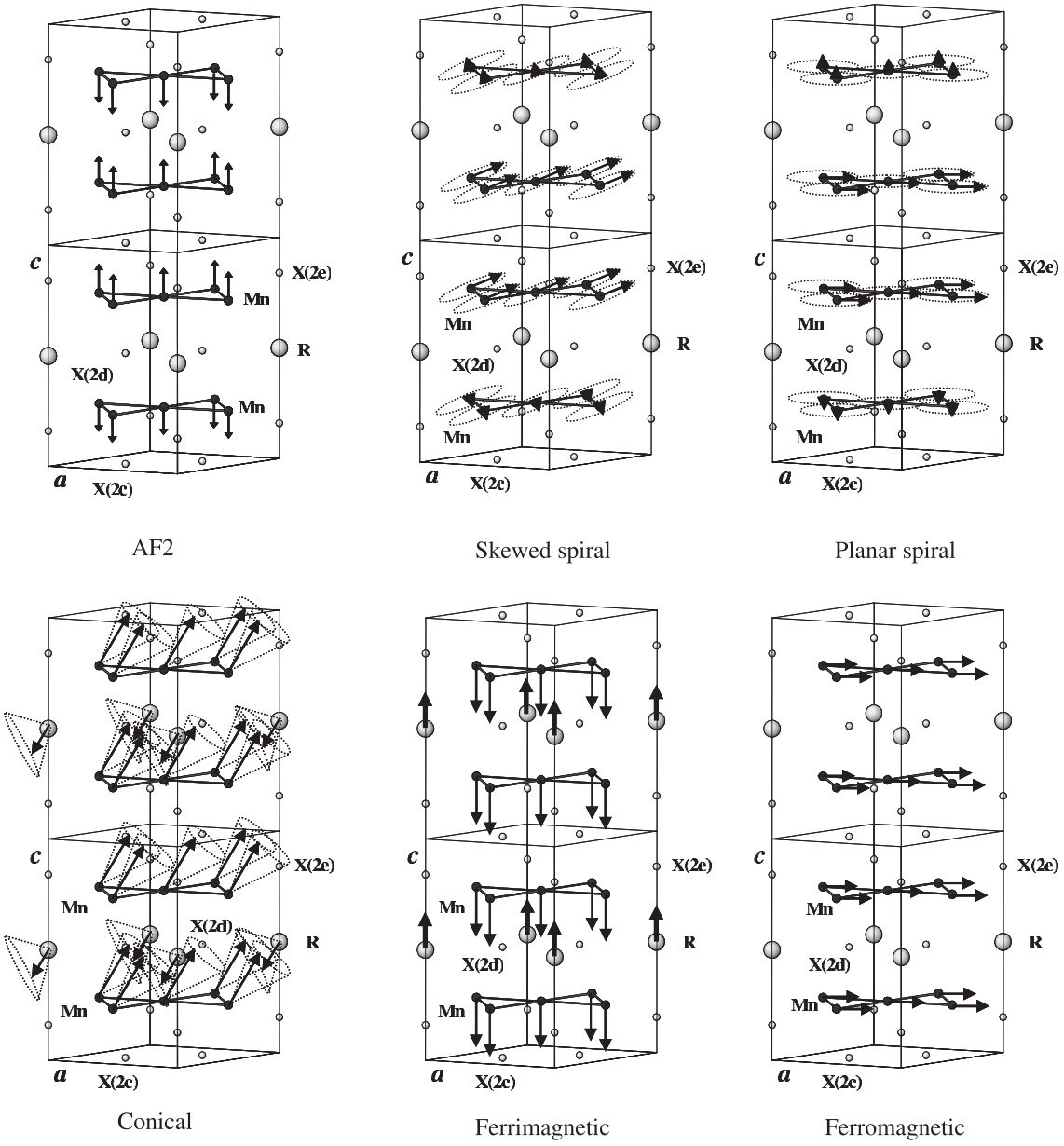

Figure 4. Schematic representation of the various magnetic structures in $YbMn_6Ge_{6-x}Sn_x$.

Table 1. Refined magnetic parameters of $YbMn_6Ge_{5.7}Sn_{0.3}$ from neutron diffraction data at 300 and 2 K. R_n and R_m are the Bragg agreement factors calculated for, respectively, the nuclear and magnetic contribution to the diffraction pattern while R_{wp} is the weighted profile Rietveld agreement factor.

T (K)	q_z (r.l.u.)	m_{Mn} (μ_B)	m_{Yb} (μ_B)	θ (deg)	φ (deg)	α_{Mn} (deg)	α_{Yb} (deg)	R_n, R_m, R_{wp} (%)
300	1/2	1.63(24)	—	—	—	—	—	7.5, 13.4, 18.3
2	0.244(1)	2.07(19)	2.89(37)	66(4)	172(4)	61(8)	117(14)	7.0, 16.5, 19.3

3.2.2. Alloys with $3.2 \leqslant x \leqslant 3.8$. Intermediate solid solution alloys can be subdivided into two groups. The alloys with $3.2 \leqslant x \leqslant 3.8$ initially order antiferromagnetically, with Néel temperatures ($T_N \sim 340$ K) significantly lower than those of the alloys of the Ge-rich terminal solid solution, then enter a state with a spontaneous magnetization below about $T_t \sim 35$ K (figure 5). In addition to the ferromagnetic ordering of the $Mn_5Ge_{3-x}Sn_x$ impurity, particularly visible for the $x = 3.2$ border composition, the thermomagnetization curves also present a weak anomaly near 130 K which might be related to changes in the magnetic structure.

Between 300 and 2 K, the neutron diffraction patterns of $YbMn_6Ge_{2.2}Sn_{3.8}$ (figure 6) include a set of magnetic satellites which can be indexed with an incommensurate wave vector $\mathbf{k} = \langle 0, 0, q_z \rangle$ which depends weakly on temperature ($q_z \sim 0.25$ r.l.u.). Two magnetic transitions, corresponding

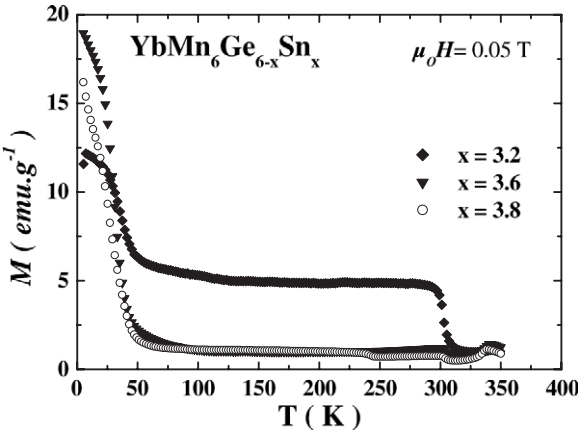

Figure 5. Temperature dependence of the magnetization of $YbMn_6Ge_{6-x}Sn_x$ ($x = 3.2$, 3.6 and 3.8).

to modification in the intensity of the magnetic satellites, can be distinguished at ∼130 and ∼40 K, in good agreement with the temperature dependence of the magnetization. From 300 K down to 130 K, the best refinements are obtained using a planar helimagnetic arrangement of the Mn sublattice built out of ferromagnetic (001) Mn planes, similar to that found in RMn_6Sn_6 with non-magnetic trivalent R (R = Sc, Y, Lu) [23, 24]. The cone half-angle is $\alpha_{Mn} = 90°$ and the angle θ between the cone axis and the c direction is 0° (figure 4). From the refined phase angle φ and q_z values, the rotation angle through the Yb-slab is found to be ∼90° while it is ∼20° through the X-slab, i.e. nearly ferromagnetic (see [24] for details). The room temperature magnetization curves (figure 7) are characterized by a metamagnetic transition with a critical field of ∼1.5 T, showing that this helimagnetic arrangement can be easily destabilized by an applied magnetic field. Below ∼130 K, a net decrease in the intensity of some magnetic satellites arises from a reorientation of the plane of the Mn spiral, so that it deviates significantly from the basal plane. However, there is no magnetic ordering of the Yb sublattice. At 110 K, the angle θ between the cone axis and the c direction refines to 89(10)°. The magnetic structure is then a skewed spiral or a cycloid spiral if θ is strictly equal to 90° (figure 4). Below ∼40 K, it is necessary to include a magnetically ordered Yb sublattice to fit the neutron diffraction data. The best refinements (table 2) were obtained using a conical arrangement similar to that of $YbMn_6Ge_{5.7}Sn_{0.3}$, but for $YbMn_6Ge_{2.2}Sn_{3.8}$ the cone axis is collinear with the [001] direction (i.e. $\theta = 0°$) and the cone formed by the Yb magnetic moments is so open that they almost lie in the basal plane [$\alpha_{Yb} = 94(10)°$]. At 2 K, the Mn moment magnitude is refined to $m_{Mn} = 2.23(8)\ \mu_B$. The Yb moment $m_{Yb} = 1.75(22)$ is both below its free ion value and somewhat lower than that found in $YbMn_6Ge_{5.7}Sn_{0.3}$. At 5 K, the field dependence of the magnetization appears mostly ferromagnetic with a low initial susceptibility but it fails to saturate even in an applied field of 5 T (figure 7). Except for the impure $x = 3.2$ sample, the magnetization remains well below the ∼12 μ_B/f.u. expected for a simple ferromagnetic order of the Mn sublattice, consistent with the occurrence of Yb moments ordered antiparallel to the Mn sublattice.

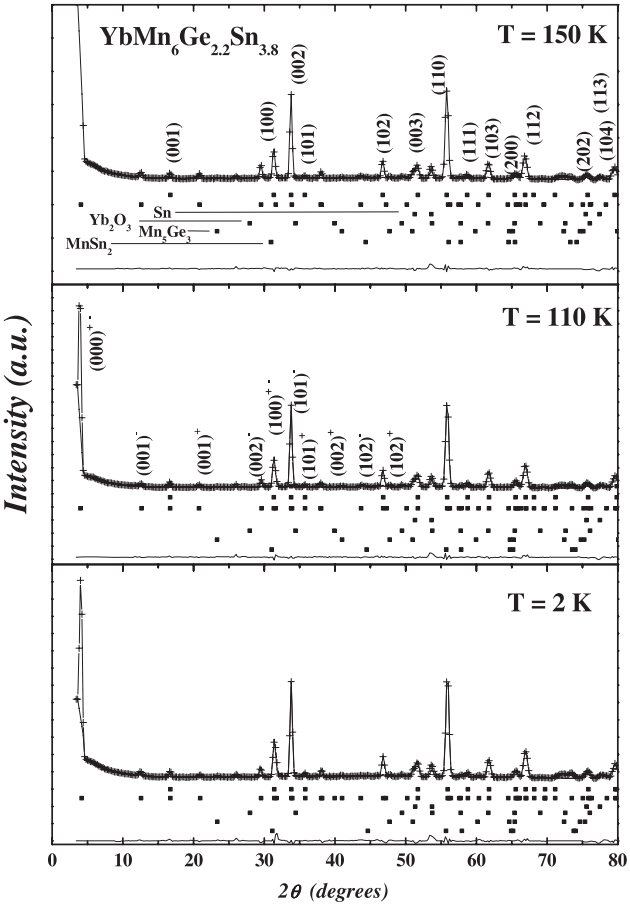

Figure 6. Neutron diffraction patterns of $YbMn_6Ge_{2.2}Sn_{3.8}$ at 150, 110 and 2 K.

3.2.3. Alloys with $4.0 \leqslant x \leqslant 4.6$. In this concentration range, the alloys initially order ferromagnetically ($T_C \sim$ 335 K) with a substantial magnetization (figure 8, left panel) and a strong out-of-phase contribution to the AC susceptibility (figure 8, right panel). Further cooling leads to the formation of a low-magnetization state (i.e. antiferromagnetic-like) below T_{AF} (figure 8, left panel). The temperature extent of the ferromagnetic state significantly widens with increasing Sn content ($T_{AF} = 315$ K for $x = 4.0$; $T_{AF} = 243$ K for $x = 4.6$). In some cases, minor anomalies are seen in the thermomagnetization curves near 120 K. At much lower temperatures, a spontaneously magnetized state re-emerges with a transition temperature which strongly increases with increasing Sn content (from ∼55 K for $x = 4.0$ up to ∼110 K for $x = 4.6$). At 300 K, the field dependence of the magnetization is of ferromagnetic type, and both the initial susceptibility and the maximum magnetization recorded at 5 T increase with the Sn content (figure 9).

The neutron diffraction pattern of $YbMn_6Ge_{1.8}Sn_{4.2}$ recorded at 320 K (figure 10) shows that this alloy is a simple basal plane collinear ferromagnet as in RMn_6Sn_6 with divalent R (R = Mg, Ca, Yb) [20, 22] or as in $MgMn_6Ge_6$ at high temperatures [27]. Below about 305 K, the intensity of the ferromagnetic peaks goes to zero while a set of incommensurate magnetic reflections appears. These satellites

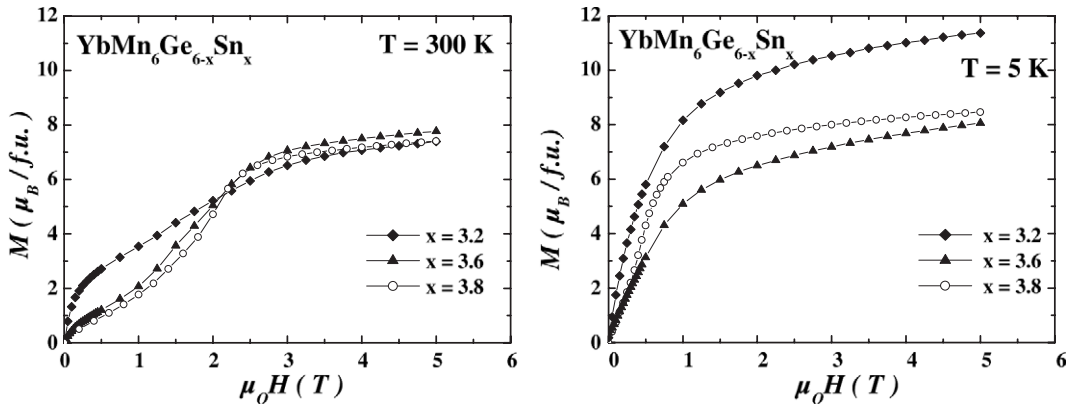

Figure 7. Field dependence of the magnetization of $YbMn_6Ge_{6-x}Sn_x$ ($x = 3.2$, 3.6 and 3.8) at 300 and 5 K.

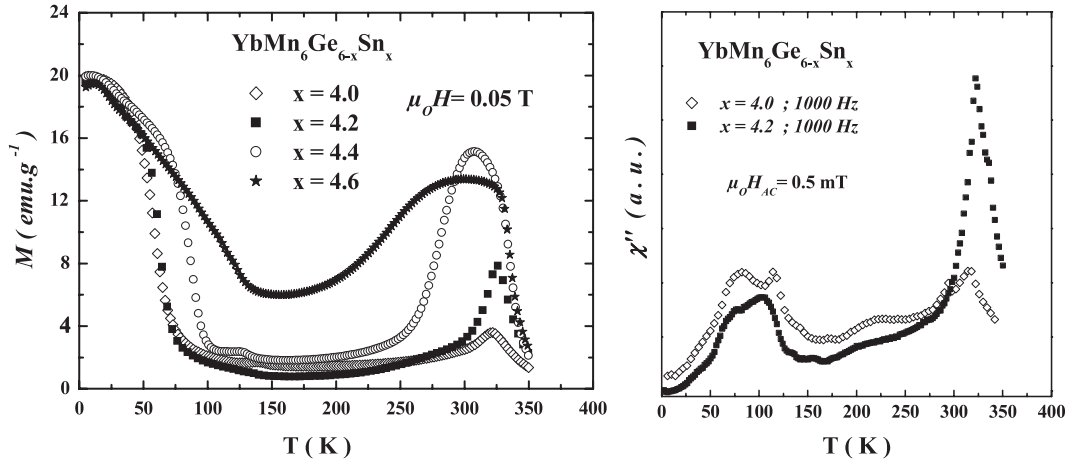

Figure 8. Temperature dependence of the magnetization of $YbMn_6Ge_{6-x}Sn_x$ ($x = 4.0$, 4.2, 4.4 and 4.6), left panel. Temperature dependence of the imaginary part of the susceptibility of $x = 4.0$ and 4.2, right panel.

Table 2. Refined magnetic parameters of $YbMn_6Ge_{2.2}Sn_{3.8}$ from neutron diffraction data at 290, 150, 110 and 2 K.

T (K)	q_z (r.l.u.)	m_{Mn} (μ_B)	m_{Yb} (μ_B)	θ (deg)	φ (deg)	α_{Mn} (deg)	α_{Yb} (deg)	R_n, R_m, R_{wp} (%)
290	0.254(1)	1.32(5)	—	0	41(8)	90	—	4.5, 17.7, 14.1
150	0.245(1)	2.08(4)	—	0	39(4)	90	—	3.4, 11.6, 10.7
110	0.242(1)	2.22(6)	—	89(10)	39(2)	90	—	3.3, 15.3, 11.5
2	0.248(1)	2.23(8)	1.75(22)	0	199(5)	54(3)	94(10)	4.0, 22.2, 13.5

Table 3. Refined magnetic parameters of $YbMn_6Ge_{1.8}Sn_{4.2}$ from neutron diffraction data at 320, 150, 100 and 2 K.

T (K)	q_z (r.l.u.)	m_{Mn} (μ_B)	m_{Yb} (μ_B)	θ (deg)	φ (deg)	α_{Mn} (deg)	α_{Yb} (deg)	R_n, R_m, R_{wp} (%)
320	0	0.93(12)	—	—	—	—	—	4.5, 9.1, 8.2
150	0.213(1)	1.56(3)	—	0	40(4)	90	—	7.6, 3.1, 10.4
100	0.216(1)	2.19(6)	—	86(17)	37(2)	90	—	3.0, 14.4, 14.8
2	0	2.36(8)	1.67(8)	—	—	—	—	3.6, 1.9, 6.9

can be fitted by considering a propagation vector $\mathbf{k} = \langle 0, 0, q_z \rangle$ with $q_z \sim 0.21$ r.l.u (table 3). Their intensity increases smoothly down to ∼115 K, at which temperature the intensity of the (00l) satellites abruptly falls without a noticeable change in the q_z component. Between 305 and 115 K, the magnetic structure is the planar spiral previously described (section 3.2.2). Below 115 K, the plane of the spiral reorients towards the c axis and, at 100 K, the angle θ between the plane of the spiral and the c axis is refined to 86(17)°. This skewed spiral (or cycloid spiral) is stable down to about 60 K where, in contrast with what was found in $YbMn_6Ge_{2.2}Sn_{3.8}$, the incommensurate satellites disappear completely and magnetic intensity appears on top of some nuclear reflections. The magnetic periodicity is then identical to the chemical one and, since the magnetic intensities of the (00l) Bragg peaks are all zero, the magnetic moments

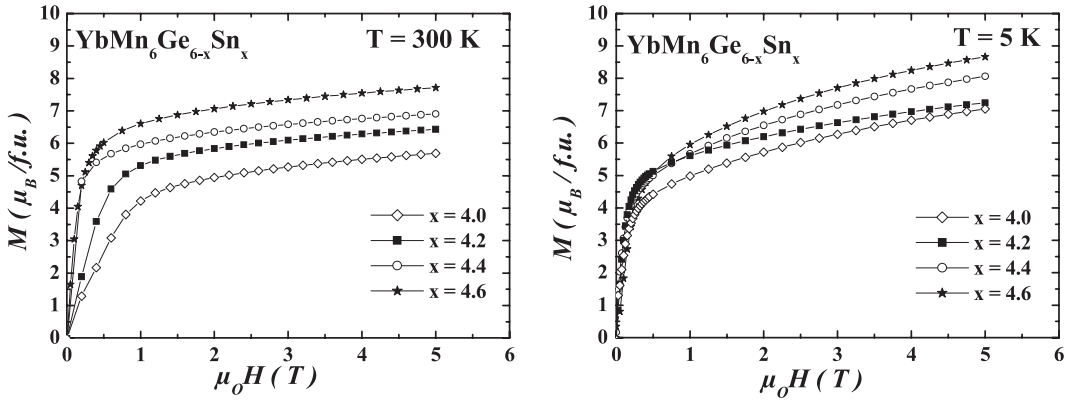

Figure 9. Field dependence of the magnetization of $YbMn_6Ge_{6-x}Sn_x$ ($x = 4.0$, 4.2, 4.4 and 4.6) at 300 and 5 K.

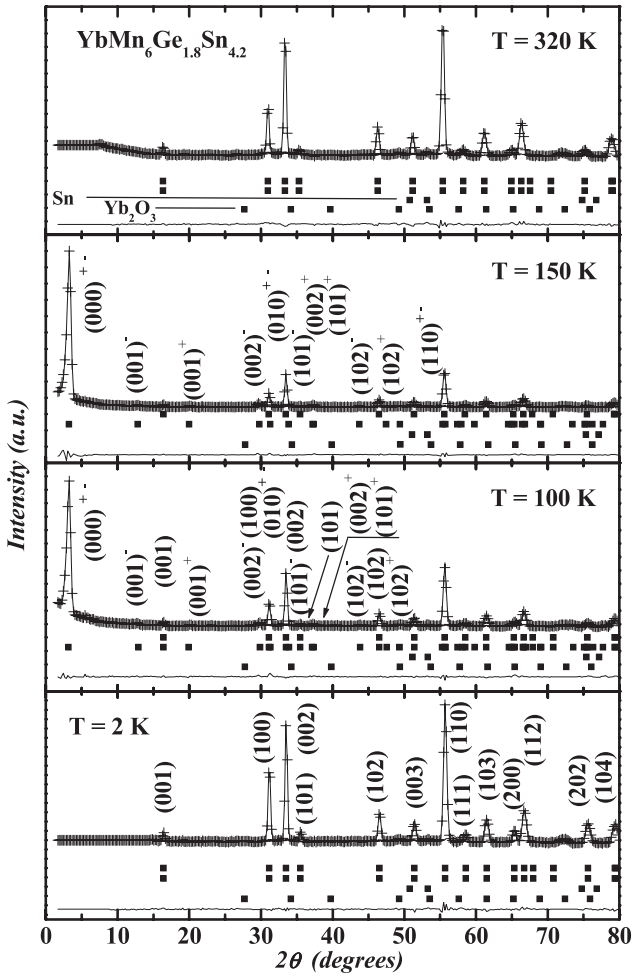

Figure 10. Neutron diffraction patterns of $YbMn_6Ge_{1.8}Sn_{4.2}$ at 320, 150, 100 and 2 K.

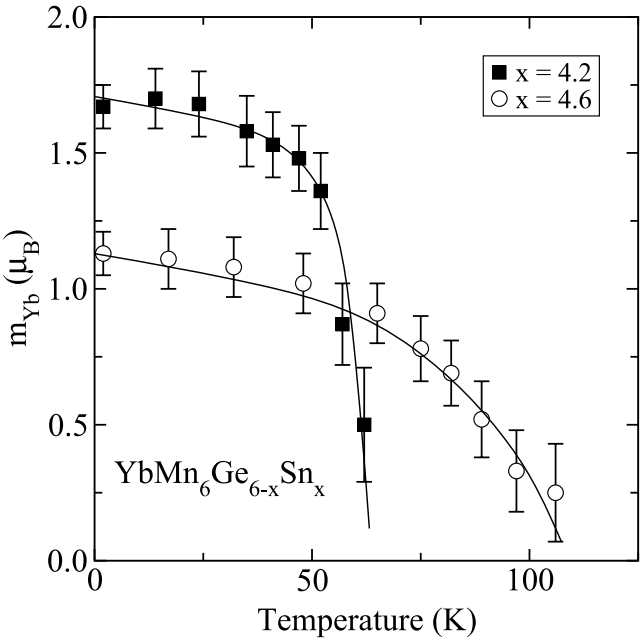

Figure 11. Thermal variation of the Yb moment magnitude in the ferrimagnetic state of the alloys with $x = 4.2$ and 4.6.

are directed along the c axis. Refinements unambiguously show that the Yb sublattice is also magnetically ordered. Below 60 K, a state with a net magnetization re-emerges (figure 8, left panel) and $YbMn_6Ge_{1.8}Sn_{4.2}$ becomes a collinear ferrimagnet built out of ferromagnetic (001) Mn and Yb layers that are antiferromagnetically coupled (figure 4). At 2 K the Mn moment magnitude is $m_{Mn} = 2.36(4)\ \mu_B$ while the Yb moment is $m_{Yb} = 1.67(8)\ \mu_B$, even lower than in the more Ge-rich alloys. Neutron data were also recorded for $YbMn_6Ge_{1.4}Sn_{4.6}$ for temperatures below 150 K. Refinements of the neutron patterns again clearly show that the low temperature magnetized state below about 110 K (figure 8, left panel) is due to the ferrimagnetic arrangement of the Mn and Yb moments. The Yb moment is still reduced and it is refined to $m_{Yb} = 1.13(8)\ \mu_B$. The temperature dependence of the Yb moment in the ferrimagnetic state of the alloys with $x = 4.2$ and 4.6 is shown in figure 11. The field dependence of the magnetization at 5 K (figure 9) supports this ferrimagnetic ordering: the initial susceptibility is high and the ~8 μ_B/f.u. maximal magnetization, though not saturated, agrees well with a Yb moment antiparallel to the Mn moments. For $x = 4.0$ and 4.4, the low temperature increase in the magnetization associated with the magnetic ordering of the Yb sublattice takes place at ~55 K and ~90 K, respectively. These are remarkably high ordering temperatures for ytterbium

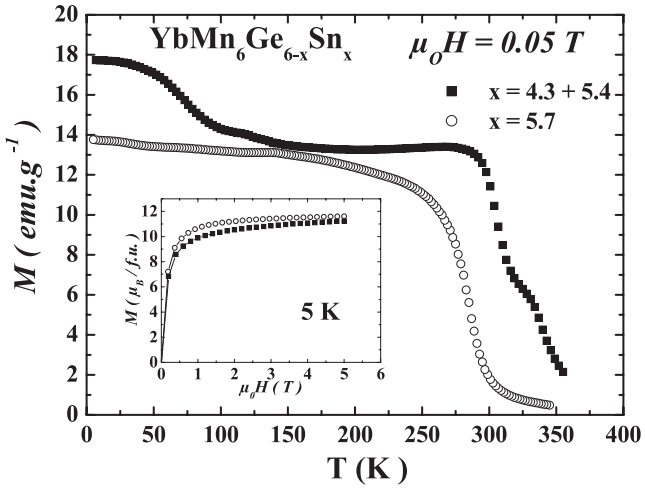

Figure 12. Temperature dependence of the magnetization of $YbMn_6Ge_{0.3}Sn_{5.7}$ and of the mixed sample $x = 5$ annealed at 650 °C. The inset shows the field dependence of the magnetization at 5 K.

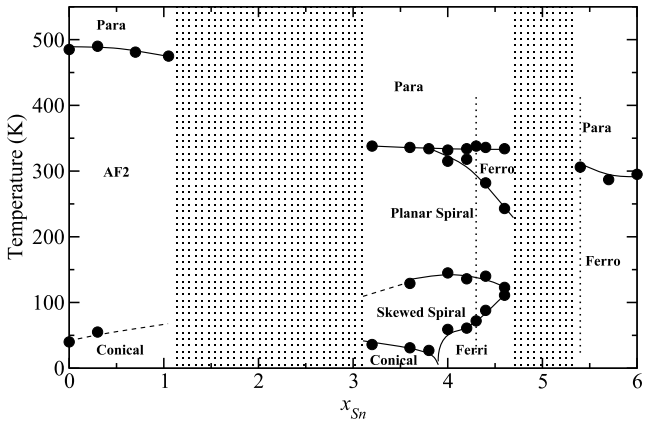

Figure 13. (x, T) magnetic phase diagram of $YbMn_6Ge_{6-x}Sn_x$. The vertical dotted lines mark compositions from the $x = 5.0$ two-phase sample.

(up to 110 K), and it is likely that exchange coupling to the ordered Mn sublattice plays a major role. Remarkably, on increasing the Sn content from $x = 4.0$ to 4.6, the Yb ordering temperature is found to increase, despite the clear decrease in Yb moment and the increase in interatomic distances. In addition, the Yb ordering temperatures for the alloys with $4.0 \leqslant x \leqslant 4.6$ are similar to, or higher than, the ordering temperature of Tm in $TmMn_6Ge_2Sn_4$ (∼70 K) [32], indicating a deviation from de Gennes scaling [36]. Reduced rare-earth magnetic moments compared to their free ion values and breakdown of de Gennes scaling are often the result of crystal field effects [37]. However, in $YbMn_6Ge_{6-x}Sn_x$ with $4.0 \leqslant x \leqslant 4.6$ the Mn sublattice provides a strong exchange field at the Yb site which should limit the influence of the crystal field. In addition, we note that in other $RMn_6Ge_2Sn_4$ alloys (R = Tb, Ho or Tm), the R atoms carry magnetic moments that are close to their expected free ion values [32, 33], and they do not appear to be significantly affected by crystal field effects. Furthermore, de Gennes scaling relies on the assumption of a similar band structure throughout a given series [36, 38]. However, the presence of non-trivalent Yb must affect the band structure, violating this assumption, so that deviations from a simple de Gennes scaling of ordering temperatures are to be expected. Hence, the reduced Yb moments and abnormally high Yb magnetic ordering temperatures in $YbMn_6Ge_{6-x}Sn_x$ ($4.0 \leqslant x \leqslant 4.6$) could be the result of the Yb being of intermediate valence.

3.2.4. Alloys with $x \geqslant 5.3$. $YbMn_6Ge_{0.3}Sn_{5.7}$, like $YbMn_6Sn_6$ [20], is a simple ferromagnet (figure 4) over the whole ordered temperature range, with a Curie temperature of $T_C \sim 287$ K (figure 12). The thermomagnetization curve of the mixed sample (initial composition $x = 5.0$, annealed at 650 °C) composed of a mixture of $x = 4.3$ and 5.4 is also presented in figure 12. Its thermomagnetic behaviour is a superposition of those of $x = 4.3$ and 5.4. The high temperature ferromagnetic ordering ($T_c \sim 338$ K) and the low temperature ferrimagnetic order (72 K) observed at the Sn-rich end of the intermediate solid solution are both apparent, as is the ferromagnetic ordering near room temperature ($T_C \sim 305$ K) of the Sn-rich terminal solid solution. The inset in figure 12 shows the field dependence of the magnetization at 5 K. The maximal magnetization of ∼12 μ_B/f.u. points to a simple collinear ferromagnetic arrangement of the Mn moments.

3.2.5. (x, T) magnetic phase diagram and its interpretation. The (x, T) magnetic phase diagram presented in figure 13 was constructed using our magnetization and neutron results. The data for $x = 0$ and 6 were taken from [18, 20]. The magnetic phase diagram is quite complex and comprises six distinct magnetic structures sketched in figure 4. If we examine the low temperature part of the phase diagram, we can start to develop a picture of the Yb valence behaviour. For the alloys with $x \leqslant 4.6$, the Yb magnetic sublattice is found to be magnetically ordered at relatively high temperatures (up to ∼110 K) with a substantial magnetic moment, (although this is somewhat reduced when compared to the free ion value), suggesting that the Yb is trivalent. In contrast, both the ferromagnetic Mn sublattice and the lack of Yb magnetic ordering for the alloys with $x \geqslant 5.3$ strongly indicate that the Yb is divalent in this composition range. This description of the Yb valence state in $YbMn_6Ge_{6-x}Sn_x$ based on the low temperature magnetic behaviour agrees fully with the interpretation of the cell volumes (figure 1, top panel) taken from room temperature x-ray diffraction data (section 3.1).

However, the situation becomes more puzzling when one considers the high temperature magnetic behaviour. Ferromagnetism of the Mn sublattice is observed for $x \geqslant 4.0$ but, as outlined earlier, a ferromagnetic Mn sublattice in RMn_6X_6 (X = Ge or Sn) is always associated with divalent R atoms whereas trivalent R atoms always yield antiferromagnetism. Stabilizing ferromagnetism in non-magnetic trivalent R compounds typically requires the partial replacement of the tetravalent Sn or Ge metalloid by a trivalent one (Ga or In) so as to decrease the average valence electron

concentration (see, for instance, [39, 40]). This tends to suggest that the high temperature Mn ferromagnetism observed in the alloys with $4.0 \leqslant x \leqslant 4.6$ may be due to the Yb not being fully trivalent. It must also be noted that the antiferromagnetism of the Mn sublattice seems to be already weakened for $3.2 \leqslant x \leqslant 3.8$, since these alloys show metamagnetic transitions in low magnetic field, while inducing a metamagnetic transition in ternaries RMn_6X_6 (X = Ge or Sn) needs significantly stronger magnetic fields [39, 41, 42]. A weakening of the Mn–Mn interlayer antiferromagnetic interaction has been reported for $RMn_6Ge_2Sn_4$ [31] although it was incomplete and did not lead to ferromagnetic order in zero field. Taken together, these observations suggest that there is a more gradual evolution of the Yb valence with composition than the simple step inferred from the x-ray data and the low temperature magnetic behaviour. However, the early departure from trivalent Yb cannot be too large as there are no significant changes in the cell volume until $x \geqslant 5.3$.

If we assume that Yb is not fully trivalent for $4.0 \leqslant x \leqslant 4.6$, at least at high temperatures, the observation of magnetic order at the Yb sites at low temperatures represents an unusual physical phenomenon. If this low temperature order is, as in most cases, due to fully trivalent Yb, then the Yb valence must have increased upon cooling, even though low temperatures generally favour the divalent form [12–14]. The increase of the Yb valence might be due to the thermal contraction. Alternatively, if the Yb valence does not vary significantly with temperature and the low temperature magnetic ordering does indeed involve intermediate valence Yb carrying a significant magnetic moment, then we are faced with an as yet unreported and somewhat unexpected situation. The abnormally high magnetic ordering temperature of Yb, which could involve partially delocalized f electrons [3, 4], suggests that the Yb behaviour is not that of a simple trivalent atom.

3.3. ^{170}Yb Mössbauer spectroscopy

The spectrum of the $YbMn_6Ge_{5.7}Sn_{0.3}$ sample shown in figure 14 exhibits the characteristic pattern of five well-separated lines reflecting a significant hyperfine field at the ^{170}Yb nucleus. Fitting the spectrum yields a hyperfine field (B_{hf}) of 281(2) T. If we assume that this field is due entirely to the local moment on the ytterbium atom and use the established conversion factor of 100 T/μ_B [43], this implies an ytterbium moment of 2.81(2) μ_B. This is in excellent agreement with the 2.89(37) μ_B derived from the analysis of the neutron scattering data presented earlier. The second parameter that can be obtained from our analysis of the ^{170}Yb Mössbauer spectrum is the quadrupole interaction parameter (eQV_{zz}), which is the product of the quadrupole moment of the 84.25 keV excited state of the ^{170}Yb nucleus ($Q = 2.0(1)$ b) and the principal component of the electric field gradient tensor (V_{zz}). The Yb^{3+} ion is non-spherical due to the presence of a single hole in its 4f shell, so a large value for eQV_{zz} is expected. In contrast, the Yb^{2+} ion has a closed 4f shell, and so is spherically symmetric. As a result, the observed electric field gradient derives primarily from contributions of the surrounding atoms. Thus, $eQV_{zz}^{Yb^{2+}} \ll eQV_{zz}^{Yb^{3+}}$. We note in passing that the

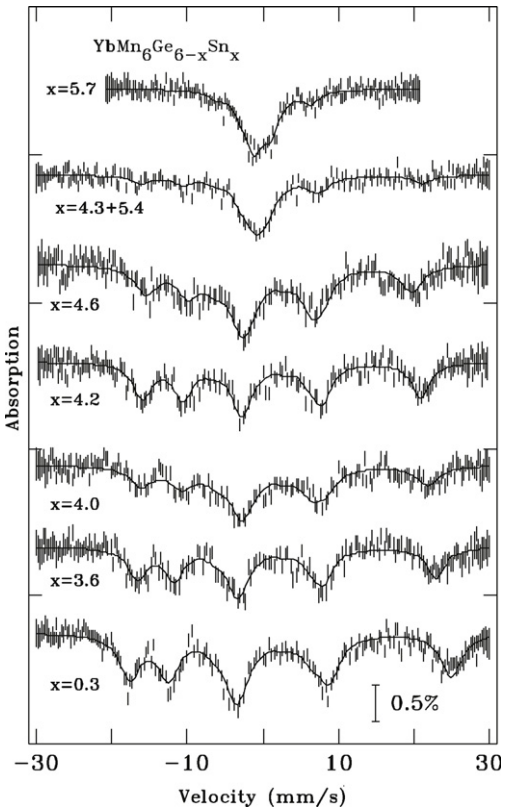

Figure 14. ^{170}Yb Mössbauer spectra for $YbMn_6Ge_{6-x}Sn_x$ at 5 K. There is a clear evolution from the widely split magnetic pattern for low x to a simple non-magnetic central feature by $x = 5.7$.

$2^+ \rightarrow 0^+$ transition used for ^{170}Yb Mössbauer spectroscopy is primarily rotational in nature. It does not involve a significant nuclear size change and so the isomer shift that is diagnostic of valence in ^{57}Fe and ^{151}Eu Mössbauer spectroscopy (for example) is essentially zero for ^{170}Yb and does not generally yield useful information. The spectrum for $YbMn_6Ge_{5.7}Sn_{0.3}$ shown in figure 14 indicates that the ytterbium is trivalent and magnetically ordered at 5 K.

Ytterbium occupies a single site in the $HfFe_6Ge_6$-type structure, and the five lines that occur in a magnetically split single-site ^{170}Yb Mössbauer spectrum should have equal intensities. However, it is clear that the two absorption lines either side of zero velocity in the $YbMn_6Ge_{5.7}Sn_{0.3}$ spectrum shown in figure 14 are more intense than the other three lines in the pattern. This is due to the presence of the Yb_2O_3 impurity noted earlier. Analysis of the spectra including this component shows that it accounts for about 20% (but as much as 40% in some cases) of the spectral area, which would seem to be inconsistent with the few wt % detected by x-ray diffraction. However, ^{170}Yb Mössbauer spectroscopy sees *only* the ytterbium atoms in each phase, and Yb_2O_3 has a higher mass fraction of ytterbium than $YbMn_6Ge_{6-x}Sn_x$ does (∼88% versus ∼16%), making Mössbauer spectroscopy more than five times more sensitive to the presence of Yb_2O_3 than it is to $YbMn_6Ge_{6-x}Sn_x$. A second factor affecting the observed intensity is that the spectral weight of each component is scaled by the probability that the absorption of the γ photon occurs

without recoil—the Lamb–Mössbauer or f factor. For the 14.4 keV γ used for ^{57}Fe Mössbauer spectroscopy, the f-factor correction is rarely an issue, but it becomes more significant with increasing energy, and by the 84.25 keV energy used here, it is a major concern. Indeed, the thermal contribution to the f factor limits our useable temperature range to below 50 K for ^{170}Yb Mössbauer spectroscopy. As a refractory oxide Yb_2O_3 has a hard lattice that is reflected in its Debye temperature (θ_D) of about 280 K [44]. In contrast, the RMn_6Sn_6 intermetallics tend to be much softer materials with Debye temperatures of the order of 100 K [45]. For measurements made well below θ_D as here, this difference in Debye temperature leads to a factor of ten difference in the f factor between Yb_2O_3 and $YbMn_6Ge_{6-x}Sn_x$. This easily accounts for the apparent discrepancy between the oxide contents detected by x-ray diffraction and ^{170}Yb Mössbauer spectroscopy. However, the strong Yb_2O_3 contribution does tend to obscure some of the details in the spectra of the more tin-rich samples.

As we increase the tin fraction in the compound two clear trends are evident. First, as the top panel of figure 15 shows, there is a gradual decrease in the hyperfine field, suggesting that the ytterbium moment decreases as tin is added. However, the decrease in B_{hf} is significantly smaller than the decrease in moment derived from analysis of the neutron diffraction data (15% versus over 40%, respectively). ^{170}Yb Mössbauer spectroscopy has the advantage that it sees *only* the contributions from the ytterbium in the sample, and as there are no magnetic Yb-containing impurities present (Yb_2O_3 orders at 2.3 K [44]) the measurement of B_{hf} in these samples is unambiguous and more accurate than the Yb moment magnitude derived from neutron data refinements. However, as there is no reason to expect a systematic underestimate of the ytterbium moment to develop in the neutron diffraction analysis with increasing tin content, we have to consider the possibility that the conversion factor is not composition-independent, perhaps as a result of the changing ytterbium valence (see the following).

The second clear trend shown in the lower panel of figure 15 is the marked decrease in eQV_{zz}. As the crystal structure does not change, it is unlikely that the observed decrease is being driven by changes in the lattice contribution. Furthermore, the quadrupole interaction in Yb^{3+} is expected to be dominated by local contributions from the Yb 4f shell. This leads us to the suggestion that the ytterbium valence decreases as the tin content increases above $x \sim 4.0$. This view is certainly consistent with the expansion of the Yb-slab apparent in the inset of figure 1, as a decrease in the average ytterbium valence would lead to an *increase* in the average ytterbium volume. One possibility that we can rule out immediately is the coexistence of Yb^{2+} and Yb^{3+}. We do not observe two distinct spectral components; rather we see a single, magnetically split component with both B_{hf} and eQV_{zz} decreasing steadily. The only exception to this is the $x = 5.0$ sample that was annealed at 650 °C, where we do observe two components, but this is known to be a macroscopically phase-separated sample from x-ray diffraction data. It is not possible for us to distinguish between a dynamic averaging of the ytterbium valence (i.e. some form of rapid electron hopping that leaves the ytterbium ions in an effective, time-averaged, intermediate valence state) and a truly static intermediate valence state, although, in the absence of any line broadening or lineshape changes that would indicate the presence of dynamics, we favour the static interpretation.

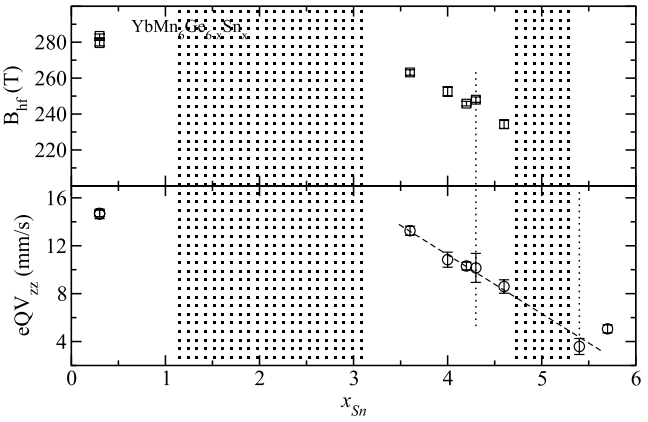

Figure 15. Composition dependence of (top) the hyperfine field (B_{hf}) and (bottom) the quadrupole interaction (eQV_{zz}) derived from fits to the ^{170}Yb Mössbauer spectra of $YbMn_6Ge_{6-x}Sn_x$ at 5 K. The shaded areas correspond to the two-phase regions. The vertical dotted lines mark compositions from the $x = 5.0$ two-phase sample, while the dotted line through the eQV_{zz} values is a simple linear fit used to interpolate values.

The change in the spectrum at $x = 5.7$ in figure 14 is quite striking. The magnetic pattern is completely gone, replaced by a poorly resolved central feature with a greatly reduced eQV_{zz}. It is interesting to note that the trend in eQV_{zz} seen in the lower tin compositions (figure 15) that were magnetically ordered continues to the non-magnetic $x = 5.7$ sample, suggesting that, while there is an abrupt change in magnetic properties, there is a gradual evolution of the (primarily) 4f contribution to eQV_{zz}. We can obtain an estimate for the lattice contribution to the quadrupole interaction by turning to data from ^{155}Gd Mössbauer spectroscopy [46, 47] and ^{159}Tb NMR [48]. Since the Gd^{3+} ion has a half-filled 4f shell, the atom is spherically symmetric and so provides no local contribution to the electric field gradient. A measurement of eQV_{zz} can therefore be converted to a determination of the lattice contribution to V_{zz} knowing the quadrupole moments of the two ^{155}Gd states used for the measurement. The values for $GdMn_6Sn_6$ are $2.0(3) \times 10^{21}$ V m^{-2} [47] and $2.0(1) \times 10^{21}$ V m^{-2} [46]. The ^{159}Tb NMR measurement yields a slightly higher estimate of $3.2(1.2) \times 10^{21}$ V m^{-2} [48], which is consistent with the ^{155}Gd data, within error. Converting our measured eQV_{zz} for the Sn-rich component of the nominal $x = 5.0$ sample[4] yields $V_{zz} = 4.8(9) \times 10^{21}$ V m^{-2}. While larger than the ^{155}Gd values, it is consistent with the ^{159}Tb NMR result, and it is possible that the lattice contribution to V_{zz} increases slightly across the series. Even if we take the lattice V_{zz} estimate from the ^{155}Gd data, it is clear that at most half of our observed quadrupole interaction could be due to the effects of the Yb

[4] While this sample was two-phased, it contained significantly less Yb_2O_3 than the $x = 5.7$ sample and the statistical quality of the pattern was superior. The reduced line overlap makes the estimate for eQV_{zz} more reliable.

4f shell, and the clear decrease in eQV_{zz} with increasing tin content seen in figure 14 must therefore reflect a reduction in the 4f contribution, suggesting a gradual evolution from trivalent Yb at $x = 0.3$ to divalent Yb by $x = 5.4$.

The change in the ^{170}Yb hyperfine field in figure 15 could come from two possible sources: (1) the Yb moment could be decreasing or (2) the transferred contribution from the neighbouring Mn moments could be decreasing. The first possibility is certainly consistent with the neutron diffraction data discussed earlier, although the moments derived from neutron diffraction appear to decrease more rapidly with increasing x than the Mössbauer hyperfine field does. An examination of the ytterbium environments allows us to rule out the second possibility. The Yb atoms in the hexagonal $HfFe_6Ge_6$-type structure have a hexagonal ring of Mn atoms above and below them. While the Mn moments are not fully parallel for the lowest temperature structures observed for $x \leqslant 3.8$, a vector sum over the Mn first neighbours yields a net contribution (see figure 4), and so a transferred field might be expected. Remarkably, for $x \geqslant 4.0$, the Mn moments form a simple ferromagnet, which should yield the maximum transferred hyperfine field, yet the observed B_{hf} continues to decrease and finally drops abruptly to zero around $x = 5$. These observations suggest that the transferred contribution to the ^{170}Yb hyperfine field is never more than a few tesla and the observed B_{hf} is dominated by the local contribution from the ytterbium moment. Both the ^{170}Yb Mössbauer data and the neutron diffraction measurements clearly show that the ytterbium moment decreases for $x \geqslant 3.2$.

Taking the trends in eQV_{zz} and B_{hf} together leads to an intriguing possibility. If we assume that the decrease in eQV_{zz} with increasing tin content reflects a steady reduction in the ytterbium valence from 3+ to 2+, and that the abrupt disappearance of the hyperfine field marks the point at which the ytterbium moment is lost, then we can combine the two datasets to determine the average valence at which the ytterbium moment collapses. Linearly interpolating between eQV_{zz} at $x = 0.3$ (magnetic, definitely Yb^{3+}) and the $x = 5.4$ value (non-magnetic, lattice expanded, assumed Yb^{2+}) and using the sample at $x = 4.6$ as the last magnetic composition, places the loss of the ytterbium moment at an average valence of about $Yb^{2.4+}$. Using the ^{155}Gd Mössbauer value as the lattice contribution that should mark the fully divalent ytterbium state moves our estimate for the magnetic/non-magnetic boundary up to $Yb^{2.5+}$, but does not materially affect our conclusion that the ytterbium ion carries a significant moment well into the intermediate valence regime.

Finally, there is a severe breakdown in the expected scaling between the observed hyperfine field and the measured ytterbium moments for $3.6 \leqslant x \leqslant 4.6$. The scaling failure occurs in the same composition range that the ytterbium valence is changing, suggesting that this may be another effect of the valence change. While the factor of two change in scale factor appears rather large, it is well outside any possible error source. We are not aware of any other experimental results or calculations that might either support or contradict this possibility. Clearly, other magnetic systems in which the ytterbium valence changes need to be identified and investigated to fully establish the systematic behaviour of the moments and hyperfine fields.

4. Conclusions

Our combined x-ray diffraction, magnetic, neutron diffraction and ^{170}Yb Mössbauer spectroscopy study of the hexagonal $P6/mmm$ $YbMn_6Ge_{6-x}Sn_x$ system has identified three solid solution regions and a complex evolution of the magnetic properties with both composition and temperature. For $x \leqslant 4.6$, the Mn moments order above room temperature and undergo one or more reorientations on further cooling, while ordering of the Yb moments is observed between 30 and 110 K. In the terminal solid solution region ($x \geqslant 5.3$) there is no ytterbium ordering and changes in both the cell volume and the ^{170}Yb Mössbauer spectra suggest that the ytterbium is divalent in this region. The composition dependence of the magnetic and ^{170}Yb Mössbauer data suggests that there is a gradual evolution in the average ytterbium valence from Yb^{3+} at low x to Yb^{2+} at higher tin concentrations, and that the loss of ytterbium moment occurs at an average valence of ~2.5+. We find no evidence for dynamic behaviour affecting the ytterbium valence. As outlined in the introduction, magnetic ordering of intermediate valence Yb is a very rare situation [9, 10], especially at such high temperatures (up to 110 K). In $YbMn_6Ge_{6-x}Sn_x$, the very unusual high temperature magnetic ordering of intermediate valence Yb might be favoured by the strong exchange coupling to the neighbouring Mn moments, and by the fact that in RMn_6X_6 the density of states is dominated by relatively large 3d Mn contributions near the Fermi level [19, 49] that could strongly hybridize with the f peak of Yb. However, we have no direct measurement of the Yb valence and supplementary experiments are needed. Further insight into the valence behaviour of ytterbium in this complex system could come from x-ray absorption experiments, or a ^{171}Yb Mössbauer spectroscopy study, as this would be less affected by the low ytterbium content and would be able to obtain data at higher temperatures. ^{174}Yb PAC data might also be of great value by providing information on the electric field gradient, and hence the ytterbium valence, at much higher temperatures than could be accessed using Mössbauer spectroscopy. We expect that our results will stimulate further experimental and theoretical efforts for a better understanding of magnetic ordering in intermediate valence systems.

Acknowledgments

We are indebted to the Institut Laue Langevin (Grenoble, France) for the provision of research facilities. Our local contact (O Isnard) is warmly acknowledged for his assistance during the recording of the neutron patterns. We are grateful to J F Maréché (Institut Jean Lamour, Nancy, France) for machining the Mo crucibles. Parts of this work were supported by grants from the Natural Sciences and Engineering Research Council of Canada and Fonds Québécois de la Recherche sur la Nature et les Technologies. Source activations were carried out by M Butler at the McMaster Nuclear Reactor

(MNR), Hamilton, Ontario. JMC acknowledges support from the Canada Research Chairs programme.

References

[1] Iandelli A and Palenzona A 1979 *Handbook on the Physics and Chemistry of Rare Earths* vol 2 *Alloys and Intermetallics* (Amsterdam: North-Holland) p 1

[2] Lawrence J M, Riserborough P S and Parks R D 1981 *Rep. Prog. Phys.* **44** 1

[3] Temmerman W M, Szotek Z, Svane A, Strange P, Winter H, Delin A, Johansson B, Eriksson O, Fast L and Wills J M 1999 *Phys. Rev. Lett.* **83** 3900

[4] Svane A, Temmerman M, Szotek Z, Petit L, Strange P and Winter H 2000 *Phys. Rev.* B **62** 13394

[5] Stewart G R 1984 *Rev. Mod. Phys.* **56** 755

[6] Adroja D T and Malik S K 1991 *J. Magn. Magn. Mater.* **100** 126

[7] Plessel J, Abd-Elmeguid M M, Sanchez J P, Knebel G, Geibel C, Trovarelli O and Steglich F 2003 *Phys. Rev.* B **67** 180403

[8] Shah K V, Bonville P, Manfrinetti P, Wrubl F and Dhar S K 2009 *J. Phys.: Condens. Matter* **21** 176001

[9] Walter U and Wohlleben D 1987 *Phys. Rev.* B **35** 3576

[10] Bonville P, Hammann J, Hodges J A, Imbert P and Jéhanno G J 1986 *Phys. Rev. Lett.* **57** 2733

[11] Chesnut G N and Vohra Y K 1999 *Phys. Rev. Lett.* **82** 1712

[12] Pott R, Boksch W, Leson G, Politt B, Schmidt H, Freimuth A, Keulerz K, Langen J, Neumann G, Oster F, Röhler J, Walter U, Weidner P and Wohlleben D 1985 *Phys. Rev. Lett.* **54** 481

[13] Fritsch V, Thompson J D, Bobev S and Sarrao J L 2006 *Phys. Rev.* B **73** 214448

[14] Felner I and Nowik I 1986 *Phys. Rev.* B **33** 617

[15] Bauer E, Le Tuan R, Hauser R, Gratz E, Holubar T, Hilscher G, Michor H, Perthold W, Godart C, Alleno E and Hiebl K 1995 *Phys. Rev.* B **52** 4327

[16] Ryan D H, Cadogan J M and Edge A V J 2004 *J. Phys.: Condens. Matter* **16** 6129

[17] Felner I, Nowik I, Vakin D, Potzel U, Moser J, Kalvius G M, Wortmann G, Schmiester G, Hilscher G, Gratz E, Schmitzer C, Pillmayr N, Prasad K G, de Waard H and Pinto H 1987 *Phys. Rev.* B **35** 6956

[18] Venturini G, Welter R and Malaman B 1992 *J. Alloys Compounds* **185** 99

[19] Mazet T 2000 *Thesis* University of Nancy

[20] Mazet T, Welter R and Malaman B 1999 *J. Magn. Magn. Mater.* **204** 11

[21] Malaman B, Venturini G, Chafik El Idrissi B and Ressouche E 1997 *J. Alloys Compounds* **252** 41

[22] Mazet T, Venturini G, Welter R and Malaman B 1998 *J. Alloys Compounds* **264** 71

[23] Venturini G, Welter R, Malaman B and Ressouche R 1993 *J. Alloys Compounds* **200** 51

[24] Venturini G, Fruchart D and Malaman B 1996 *J. Alloys Compounds* **236** 102

[25] Schobinger-Papamantellos P, André G, Rodríguez-Carvajal J, Brabers J H V J and Buschow K H J 1995 *J. Alloys Compounds* **226** 113

[26] Mazet T, Welter R, Venturini G, Ressouche E and Malaman B 1999 *Solid State Commun.* **110** 407

[27] Mazet T, Ihou-Mouko H and Malaman B 2008 *J. Appl. Phys.* **103** 043903

[28] Rodríguez-Carvajal J 1993 *Physica* B **192** 55

[29] Voyer C J and Ryan D H 2006 *Hyperfine Interact.* **170** 91

[30] Venturini G, private communication (unpublished)

[31] Venturini G 2005 *J. Alloys Compounds* **398** 42

[32] Perry L K, Ryan D H, Venturini G and Malaman B 2009 *J. Alloys Compounds* **469** 34

[33] Venturini G, Malaman B, Perry L K and Ryan D H 2009 *J. Alloys Compounds* **484** 59

[34] Zhang Y, Runge A P, Shan Z S and Sellmyer D J 1994 *J. Appl. Phys.* **75** 6354

[35] Lefèvre C and Venturini G 2002 *J. Alloys Compounds* **340** 43

[36] de Gennes P G 1962 *J. Phys. Radium* **23** 510

[37] Noakes D R and Shenoy G K 1982 *Phys. Lett.* A **91** 35

[38] Belorizky E, Gavigan J P, Givord D and Li H S 1987 *J. Appl. Phys.* **61** 3971

[39] Zang L, Klaasse J C P, Brück E, Buschow K H J, de Boer F R, Yoshii S, Kindo K, Lefèvre C and Venturini G 2002 *Phys. Rev.* B **70** 224425

[40] Zhang S, Zhao P, Cheng Z, Li R, Sun J, Zhang H and Shen B 2004 *Phys. Rev.* B **64** 212404

[41] Matsuo A, Suga K, Kindo K, Zhang L, Brück E, Buschow K H J, de Boer F R, Lefèvre C and Venturini G 2006 *J. Alloys Compounds* **408–412** 110

[42] Koyama M, Narumi Y, Yoshii S, Kindo K, Zhang L, Brück E, Buschow K H J, de Boer F R, Lefèvre C and Venturini G 2006 *J. Alloys Compounds* **408–412** 161

[43] Abragam A and Bleaney B 1976 *Electronic Paramagnetic Resonance of Transition Ions* (Oxford: Clarendon) p 276

[44] Li H, Wu C and Ho J 1994 *Phys. Rev.* B **49** 1447

[45] Duijn H G M 2000 *PhD Thesis* Universiteit van Amsterdam, p 141

[46] Malaman B, Venturini G, Welter R, Sanchez J P, Vulliet P and Ressouche E 1999 *J. Magn. Magn. Mater.* **202** 519

[47] Dirken M W, Thiel R C, Brabers J H V J, de Boer F R and Buschow K H J 1991 *J. Alloys Compounds* **177** L11

[48] Li Y, Graham R G, Bunbury D St P, Mitchell P W, McCausland M A H, Chaughule R S, Gupta L C, Vijayaraghavan R and Godart C 1995 *J. Magn. Magn. Mater.* **140–144** 1031

[49] Mazet T, Tobola J, Venturini G and Malaman B 2002 *Phys. Rev.* B **65** 104406